JACS
JOURNAL OF THE AMERICAN CHEMICAL SOCIETY

Article

pubs.acs.org/JACS

Chemical Gating of a Synthetic Tube-in-a-Tube Semiconductor

Allen L. Ng,[†] Chien-Fu Chen,[‡] Hyejin Kwon,[†] Zhiwei Peng,[†] Cheng. S. Lee,[†] and YuHuang Wang*[,†,§]

[†]Department of Chemistry and Biochemistry, University of Maryland, College Park, Maryland 20742, United States
[‡]Institute of Applied Mechanics, National Taiwan University, Taipei, Taiwan 106
[§]Maryland NanoCenter, University of Maryland, College Park, Maryland 20742, United States

Supporting Information

ABSTRACT: A critical challenge to translating field effect transistors into biochemical sensor platforms is the requirement of a gate electrode, which imposes restrictions on sensor device architectures and results in added expense, poorer scalability, and electrical noise. Here we show that it is possible to eliminate the need of the physical gate electrode and dielectrics altogether using a synthetic tube-in-a-tube (Tube^2) semiconductor. Composed of a semiconducting single-walled carbon nanotube nested in a charged, impermeable covalent functional shell, Tube^2 allows the semiconducting conduction pathway to be modulated solely by surface functional groups in a chemically gated-all-around configuration. The removal of physical gates significantly simplifies the device architecture and enables photolithography-free, highly scalable fabrication of transistor sensors in nonconventional configurations that are otherwise impossible. We show that concomitant FET sensitivity and single-mismatch selectivity can be achieved with Tube^2 even in a two-terminal, thin film transistor device configuration that is as simple as a chemiresistor. Miniaturized two-terminal field effect point sensors can also be fabricated, using a straightforward dice-and-dip procedure, for the detection of tuberculosis biomarkers.

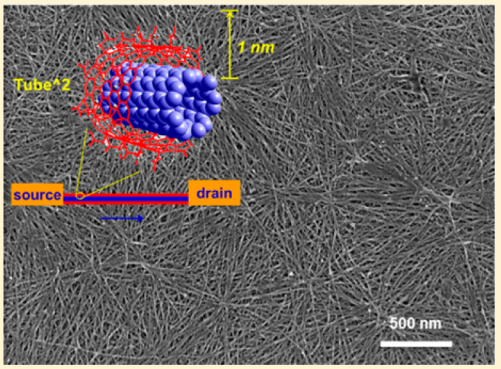

INTRODUCTION

The Information Age started with our ability to modulate current in a semiconductor by an electrical field. Exploitation of this gating effect, through chemical binding events, has generated sensitive field effect transistor (FET) sensors capable of detecting a variety of biological and chemical species.[1−5] Owing to its real-time, label-free, and miniaturized size features, electrical sensing is an attractive platform for on-site detection of viruses and protein biomarkers. Current diagnostic techniques still typically rely on methods such as polymerase chain reaction (PCR)[6] and enzyme-linked immunosorbent assays (ELISA)[7] which are time-consuming, and require sophisticated instrumentation and specialized technicians due to multistep procedures. However, a critical challenge to translating FETs into biochemical sensor platforms is the requirement of a gate electrode.[8,9] The gate electrode is used to apply an electrical potential in order to capacitively switch the semiconductor to a highly sensitive ON-state. Since the semiconductor has to be exposed to the analytes, the devices are typically gated through a back-gated electrode or an immersed electrochemical electrode. This gate electrode requirement imposes significant restrictions on sensor device architectures, limiting them typically to planar structures, and also results in added expense, poor scalability, and electrical noise.[5,10,11] On the other hand, the recent innovations in inexpensive, two-terminal nanowire and carbon nanotube (CNT) chemiresistor sensors with high sensitivity have opened up new directions for sensor development.[10,12−15]

Here we show a thin film field effect sensor composed of synthetic tube-in-a-tube (Tube^2) semiconductors, which can be electrostatically gated through chemically attached groups, eliminating the need for a physical gate electrode and dielectrics. Tube^2 is uniquely composed of a semiconducting single-walled carbon nanotube nested in a charged, impermeable covalent functional shell that allows the semiconducting conduction pathway to be modulated solely by surface receptor groups in a chemically gated-all-around configuration (Figure 1). The semiconducting channel and receptor shells are separated only by a subnanometer, van der Waals spacing. In a comparison to the conventional FET sensor device architecture, our new device architecture requires only two electrodes, source and drain, without the need of the third, gate electrode. The removal of the physical gate electrode significantly simplifies the device architecture and enables photolithography-free, highly scalable fabrication of nonconventional FET sensors. Miniaturized two-terminal point sensors are fabricated as an example to illustrate this important advantage using a simple, straightforward dice-and-dip procedure. We show that concomitant FET sensitivity and single-mismatch selectivity can be achieved with Tube^2 even

Received: November 23, 2016
Published: February 7, 2017

DOI: 10.1021/jacs.6b12111
J. Am. Chem. Soc. 2017, 139, 3045−3051

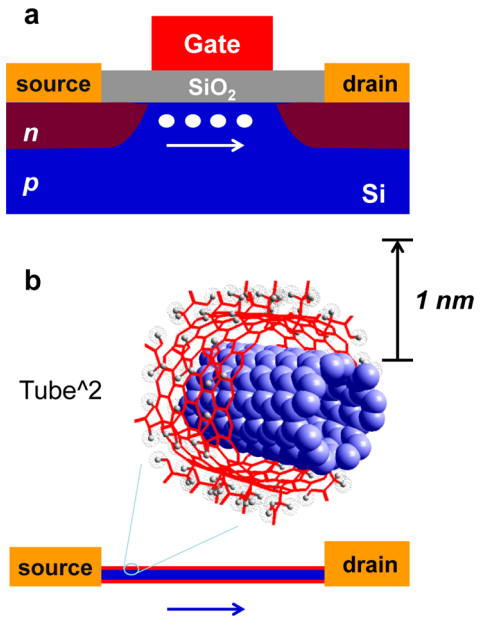

Figure 1. Schematic of chemical gating of a Tube^2 semiconductor. (a) Schematic of a conventional top-gated silicon FET. (b) A chemically gated FET based on Tube^2. Note that the gray clouded dots represent charged moieties.

in a two-terminal thin film device configuration that is as simple as a chemiresistor.

To demonstrate this gate-electrode-free detection, Tube^2 thin film transistor (TFT) sensors were created through covalent, outer-wall-selective functionalization of thin films of semiconducting double-walled carbon nanotube (DWCNT) precursors that were presorted using density gradient ultracentrifugation.[16,17] Although the major goal of this work is to demonstrate the possibility of eliminating the need for gate electrodes, the fabricated transistors can be back-gated globally using the hole-doped silicon substrate, which allows us to quantitatively compare chemical gating in Tube^2 with conventional TFT characteristics including threshold voltage (V_{th}) and carrier mobility.[18,19] Additionally, we will show it is possible to fabricate free-standing, two-terminal field effect point sensors.

MATERIALS AND METHODS

Tube^2 Thin Film Preparation. Double-walled carbon nanotubes (DWCNTs; Unidym DW411UA) were dispersed in 1 wt %/vol sodium cholate and sorted by density gradient ultracentrifugation, as reported by Hersam et al.[16] DWCNT thin films (50 mm diameter) were fabricated using a vacuum filtration method[20,21] where solutions containing 0.4 μg of DWCNTs were filtered over 50 nm pore size nitrocellulose membranes. The formed DWCNT thin films were transferred to silicon wafers with 300 nm thermal oxide coating (Silicon Quest International) through application of heat and pressure. Nitrocellulose membranes were dissolved using an acetone vapor bath, and the DWCNT film was rinsed copiously with isopropyl alcohol, ethanol, and water, followed by an annealing step at 200 °C in vacuum.

Fabrication of Microfluidic Channel-Integrated On-Chip Devices. On-chip devices were fabricated using a procedure described in our previous work.[20] Briefly, DWCNT TFTs were prepared from thin films transferred on the silicon wafers. To reduce hysteresis associated with the charge transfer from the oxide layer, a monolayer of hexamethyldisilazane was spin-coated on the substrate prior to the transfer. Channel lengths of 15 or 20 μm were defined using photolithography, with Cr/Au electrodes (10 and 75 nm thickness, respectively) deposited using electron beam deposition. Devices were characterized for conductance and transport properties using a Keithley 4200 Semiconductor Characterization System followed by an electrical breakdown step to remove metallic DWCNTs. Furthermore, polydimethylsiloxane microfluidic channels (300 × 300 μm^2 cross-section) were attached to the chip for solution introduction.

Electrochemically Accelerated Functionalization with Diazonium Salts. DWCNT TFTs were reacted with 3-fluoro-4-carboxylbenzenediazonium tetrafluoroborate electrochemically. The reagent was synthesized from 4-amino-2-fluorobenzoic acid (Sigma-Aldrich, ≥97%), fluoroboric acid, and sodium nitrite using a previously described method.[22] The diazonium structure was confirmed by ^{1}H NMR (Bruker DRX-400) and FTIR (Thermo Nicolet NEXUS 670 with ATR attachment) spectroscopies. For NMR analysis, samples were dissolved in acetonitrile-d_3 (99.8%, Cambridge Isotope Laboratories, Inc.). Covalent functionalization was achieved by flowing a 1 mM aqueous solution of 3-fluoro-4-carboxylbenzenediazonium tetrafluoroborate at a rate of 25 μL/min through microfluidic channels attached to the TFTs for 1 h. A source−drain voltage (V_{SD}) of 1 V was applied to the transistor region to electrochemically accelerate the reaction. The residual byproducts and reactants were then removed by flowing Nanopure water through the microfluidic channels for 30 min at the same flow rate. Raman spectroscopy (Horiba Jobin Yvon LabRAM Raman microscope, model ARAMIS) with an excitation line of 632.8 nm and FTIR were used to characterize the extent of covalent functionalization.

Oligonucleotide Attachment. To efficiently link amino-modified oligonucleotides to Tube^2 thin films with carboxylic acid terminal groups, 1-ethyl-3-(3-(dimethylamino)propyl)carbodiimide (EDC) and *N*-hydroxysuccinimide (NHS) were used to activate the carboxylic acid to the more reactive NHS ester terminal group. The activation experiment was performed by flowing a mixture of 20 mM EDC and 20 mM NHS at pH 5.8 at a rate of 25 μL/min through microfluidic channels attached to the TFTs for 1 h to create the NHS ester moiety. A concentration of 1 μM amino-terminated single-stranded DNA (ssDNA) in phosphate buffered saline (PBS) was then pumped through the microfluidic channels for 5 h to covalently couple the DNA to Tube^2. Unreacted ssDNA and chemicals were removed by Nanopure water pumped through the microfluidic channels for 30 min.

On-Chip Detection of Complementary Oligonucleotides. Complementary oligonucleotide detections were performed by microfluidic flow of complementary DNA (cDNA) through Tube^2 channels. Selectivity experiments were performed by flowing the noncomplementary DNA (ncDNA) sequence through TFT channel regions using the same flow rate, time, and rinsing process.

IS6110 Biomarker. Luria−Bertani (LB) plates containing standard plasmid and the IS6110 123-base fragment were obtained from the Department of Laboratory Medicine, Chang Gung Memorial Hospital, Taiwan 106. The white colonies were selected and grown in LB broth containing 50 μg/mL ampicilin in a shaker at 37 °C at 225 rpm overnight. DNA was isolated from the culture using AxyPrep Maxi Plasmid Kits and amplified using HotStar Taq DNA Polymerase to confirm the presence of the 123-base fragment. A 10 μL portion of DNA template was used in a 50 μL reaction mixture containing 0.6 μL of 25 μM primer, 4 μL of 2.5 mM dNTP, 5 μL of 5× Q solution, 5 μL of 10× buffer, 0.25 μL of 5U μL-1 HotStar Taq, and 24.55 μL of RNase-free H_2O. For PCR, the DNA was denatured at 94 °C for 15 min, followed by 35 cycles of PCR amplification when the denatured strands were annealed at 94 °C, 68 °C, and then 72 °C for 1 min each, followed by 72 °C for 10 min. The amplified products were analyzed by gel electrophoresis in 2 wt % agarose in tris-borate-EDTA buffer, mixed with fluorophore Novel Juice for visualization, and bands were visualized on a UV-light transilluminator.

The ssDNA probe for IS6110 (/5AmMC6/GC GAG CGT AGG CGT C) was covalently coupled to the carboxylic-acid-modified Tube^2 devices using the same procedure described in the oligonucleotide attachment part of this section. IS6110 was heated to 95 °C for 10 min to dehybridize the double-stranded DNA (dsDNA). The solution was quickly transported to a microfluidic injection system and flowed through the Tube^2 channel at a flow rate

DOI: 10.1021/jacs.6b12111
J. Am. Chem. Soc. 2017, 139, 3045−3051

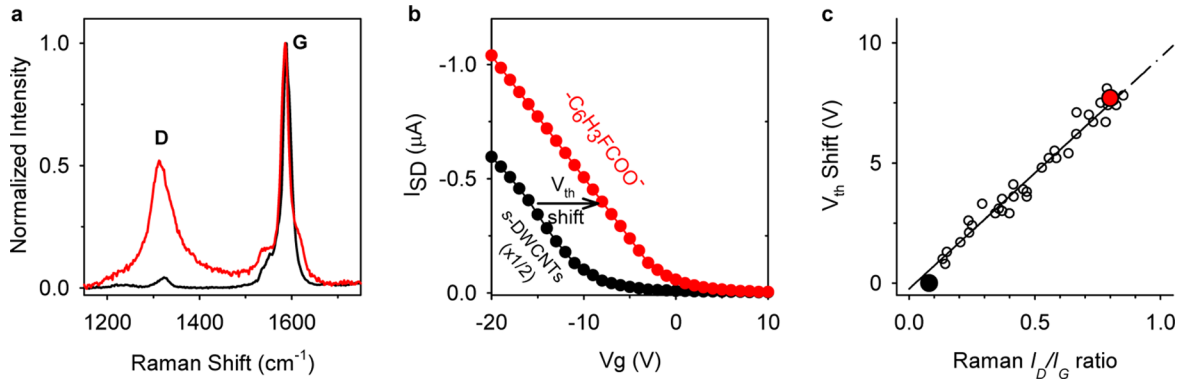

Figure 2. Chemical gating mechanism of Tube^2 thin film transistors. (a) Raman scattering of a 2-fluorobenzoic acid functionalized Tube^2 thin film (red curve) and its precursor, DWCNT (black curve). (b) Transfer characteristics of the DWCNT TFT (black; current divided by a factor of 2), and the Tube^2 TFT (red). (c) V_{th} shift as a function of Raman I_D/I_G ratio for 35 Tube^2 TFTs. The data points corresponding to the black and red curves in parts a and b are highlighted as the solid black and red dots, respectively.

of 25 μL/min. Nanopure water was then flowed through the channel to rinse off nonspecifically bound species.

Two-Terminal Field Effect Point Sensors. The Tube^2 point sensors were fabricated by a dice-and-dip procedure. We first coated both sides of an undoped Si wafers of 20 μm thickness (Virginia Semiconductor) with Cr (10 nm) for adhesion and then gold (150 nm). Afterward, the metal−silicon−metal wafer was diced into rectangular pieces (~3.5 × 0.5 mm^2). The freshly cleaved end was dipped into a 1% sodium cholate stabilized aqueous solution of DWCNTs (20 mg/L) to allow a network of Tube^2 precursors assembled across the two gold terminals. The residual surfactant was removed by Joule heating under a source−drain voltage of 5−10 V and then immersed in ethanol for 10 s; this process was repeated two additional times to remove residual surfactants or contaminants. The DWCNTs were converted to Tube^2 by immersing the device in the diazonium and then DNA solutions.

Electrical Characterization. Electrical characterization was performed on a Keithley 4200-SCS semiconductor parameter analyzer. For back-gated devices and gated measurements, transfer characteristic curves were taken after every covalent modification step to demonstrate chemical gating effects. All current versus concentration measurements, both on-chip and point sensors, were nongated with V_g = 0 V and a fixed V_{SD}.

RESULTS AND DISCUSSION

Tube^2 was synthetically created from DWCNT by outer-tube-selective functionalization with 2-fluorobenzoic acid groups using an electrochemically accelerated diazonium reaction.[23,24] Diazonium chemistry was chosen due to its outer-wall-selectivity and the tunable functionalization of aryl substituents, as demonstrated by us[20−22] and Martel et al.[25] Benzoic acid terminal groups provide concomitant versatility as a linker[26] and an abundance of negative charge at neutral pH (the pK_a of benzoic acid is ~4), which is useful for chemical gating. We found that the presence of fluorine at positions ortho relative to the carboxylic acid group improved the functional degree by ~40%. This significant improvement in functional density is attributed to reduced polymerization of the functional groups, which is known to inhibit the functionalization efficiency of diazonium reactants,[27] by the fluorine in place of an aryl hydrogen. Covalent attachment was verified through Raman spectroscopy (Figure 2a) showing the growth of the D phonon around 1300 cm^{-1}. The covalent functional degree of the Tube^2 channel was assessed using the peak area ratio of the D and G bands, which quantifies the relative ratio between sp^3 and sp^2 carbon sites, respectively. By modulating the reaction time and aryldiazonium salt concentration, various functional degrees can be achieved. Transmission peaks indicative of the covalent attachment of 2-fluorobenzoic acid were observed in the IR spectra, which include the broad carboxylic acid feature of the functional group and the absence of the diazonium peak that usually appears at 2250 cm^{-1} (Figure S1).

After outer-wall-selective covalent functionalization of DWCNTs to generate Tube^2, two approximately independent and distinct changes in the electrical transport are observed. As previously reported by us,[22] the first change is approximately a 50% decrease in conductance associated with the loss of electrical transport mobility of the outer wall. The second change results from chemical gating effects associated with the charge from the attached group[28] and can be measured as shifts in the transport properties (Figure 2b). The threshold voltage (V_{th}) shifts of functionalized DWCNT films show a strong linear correlation with the Raman I_D/I_G peak area ratios, after accounting for the loss of outer-wall-mobility (Figure 2c). We deduce that the increasing functional density of the negatively charged benzoic acid groups is generating shifts in the transport properties indicating that the dominant sensing mechanism for the Tube^2 devices is chemically driven electrostatic gating. This gating effect is a field effect similar to that in a FET, but it arises from chemical binding events rather than a gating voltage applied through a physical electrode. The mechanism of electrostatic gating is further evidenced by the ability of the Tube^2 devices to have higher sensitivity toward ammonium molecules at higher pH when the carboxylic acid groups are deprotonated (Figure S2). The ability to chemically modulate the gating environment of the Tube^2 transistor by simple tuning of the functional group and functional density allows for new opportunities to use chemically attached groups as integral gate components for the device architecture.

Unlike unfunctionalized and noncovalently modified single-walled carbon nanotube (SWCNT) transistors, we have observed that our Tube^2 devices have additional advantages such as minimal nonspecific binding to the graphitic surface (Figure S3). This improved selectivity can be attributed to the higher packing of functional groups in the outer functional shell that creates sufficient steric and electrostatic repulsion to inhibit nonspecific binding to the graphitic surface. Ruling out nonspecific binding of target and interferant compounds, we can deduce that the chemical gating of Tube^2 TFTs are predominantly a result of specifically bound functional groups.

To demonstrate the extensiveness of chemical gating in Tube^2 and its applicability toward sensing, a terminal 23-base

DOI: 10.1021/jacs.6b12111
J. Am. Chem. Soc. 2017, 139, 3045−3051

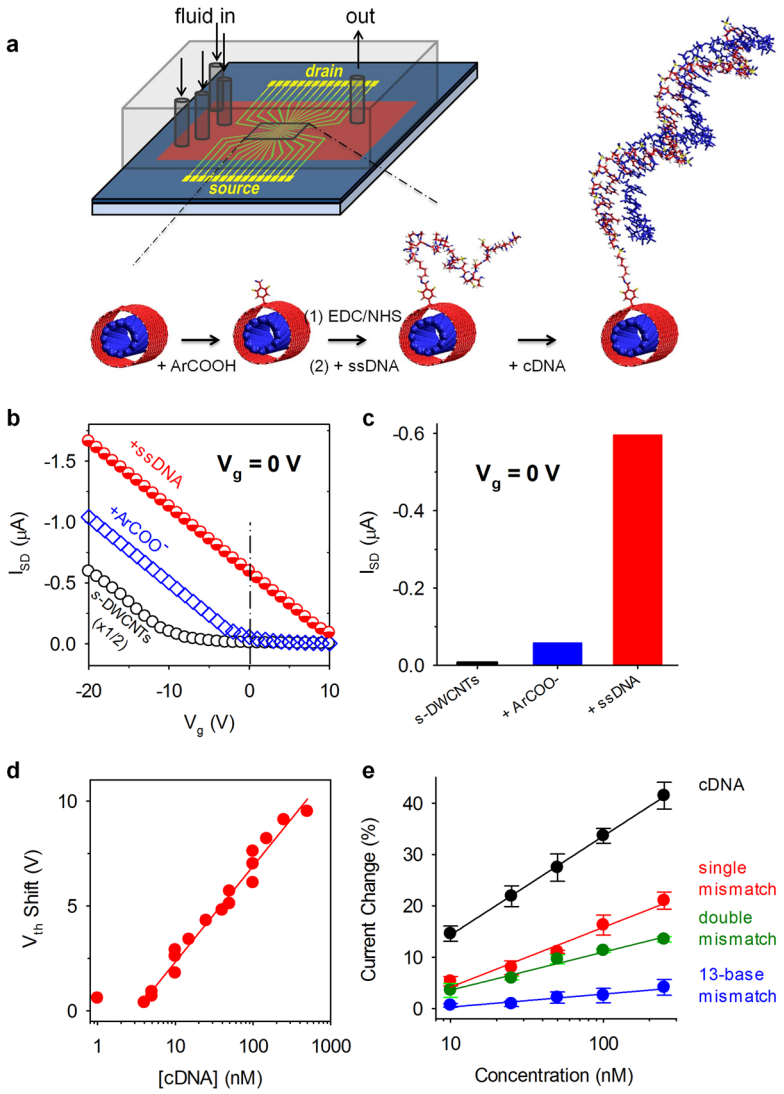

Figure 3. Gate electrode-free ssDNA TFT sensors show concomitant high selectivity and sensitivity. (a) Scheme for the preparation of a 23-base ssDNA tailored Tube^2 sensor. (b) Transport characteristics of pristine DWCNT TFT (black; current divided by a factor of 2), 2-fluorobenzoic-acid-modified Tube^2 TFT (blue), and ssDNA-modified Tube^2 TFT (red). (c) Current values of the device at V_g = 0 V, V_{SD} = −1 V, at each modification step. (d) Threshold voltage shifts as a function of cDNA concentration for nine Tube^2 devices with varying mobility. (e) Comparison of ssDNA-modified Tube^2 response when exposed to cDNA and mismatched sequences. Note that data in parts c and e were obtained through single point measurements (not I_{SD}−V_g sweep), only at V_g = 0 V (without applying a gate voltage) and V_{SD} = −1 V.

amino-modified single-stranded oligonucleotide (ssDNA) (5′-/AmMC6/ATG GTG GAT AGG CGA CTC ACG TT/-3′) was linked to the Tube^2 benzoic acid moieties for DNA detection (Figure 3a). DNA possesses a doubly negative charged phosphate group per base. With increasing oligonucleotide base length, larger electrostatic gating effects can be applied to the inner tube transducer. Upon attachment of the ssDNA, the V_{th} shifts by an additional factor of 2 compared with the fluorobenzoic acid groups and effectively turns the transistor "ON" without the use of a physical gate (Figure 3b). Accordingly, when measured without a gate (V_g = 0 V) at V_{SD} = −1 V, the conductance increases over 10 times (Figure 3c). These observations unambiguously demonstrate that chemical gating can be used as a technique to switch Tube^2 thin film devices from the OFF-state to the ON-state and can provide the same amplification effect as that achieved through gating with a conventional gate electrode.

We further show that the ssDNA tagged Tube^2 TFT under non-gated conditions can perform as well as electrode-gated TFTs. Varying amounts of the 23-base cDNA (sequence: 5′-/AAC GTG AGT CGC CTA TCC ACC AT/-3′) were added to test the sensor sensitivity (Figure 3d). All oligonucleotide solutions used for detection were prepared in 10 mM PBS. The cDNA concentration could be approximately quantified by V_{th} shifts in the electrical transport after the addition of cDNA. Nine devices with different mobilities (0.5−5.0 $cm^2/(V\,s)$), but similar functional degrees, were tested and show a strong correlation between cDNA concentration and V_{th} shift down to below 5 nM, which is comparable with three-terminal electrochemical[29] and FET sensors.[30] Upon hybridization, higher concentrations of cDNA generated larger chemical gating shifts resulting in significant modulation in the semiconductor conductance. This large chemical gating effect enables the cDNA to be electrically detected without the use of an external gate. The selectivity of ssDNA-modified Tube^2

DOI: 10.1021/jacs.6b12111
J. Am. Chem. Soc. 2017, 139, 3045−3051

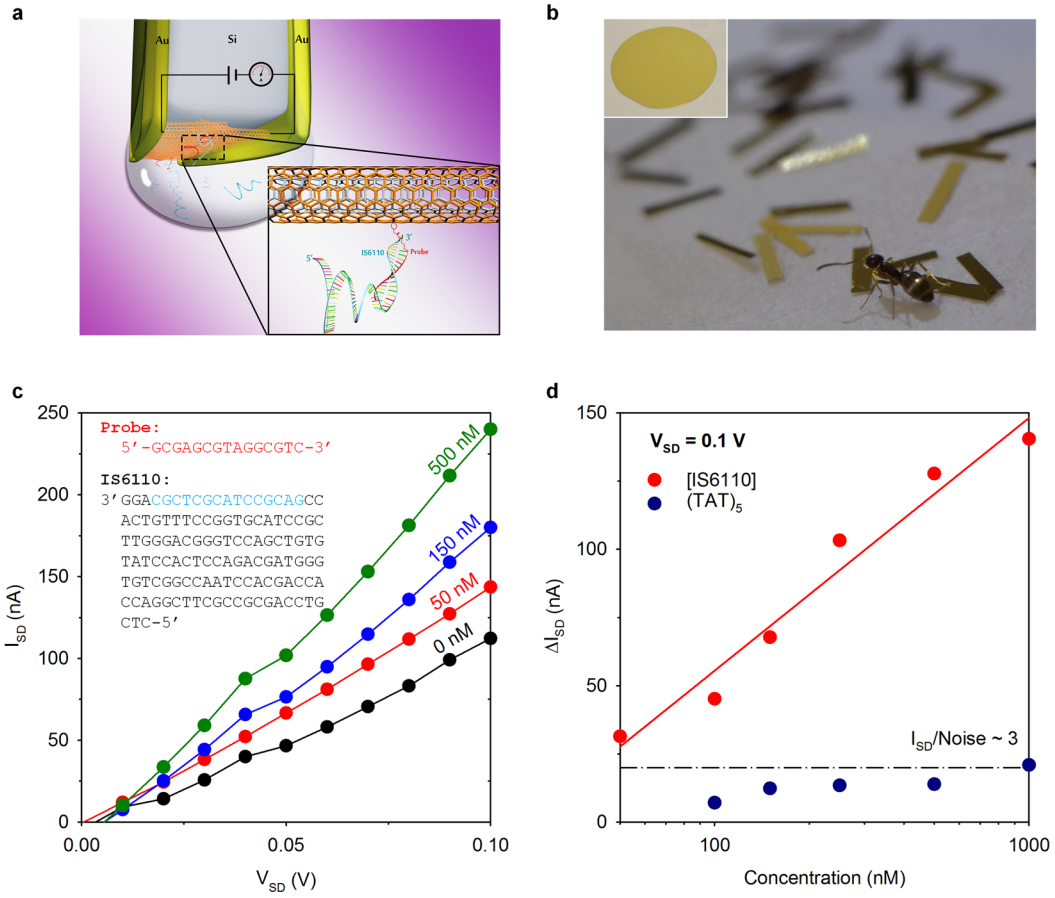

Figure 4. Tube^2 field effect point sensor for tuberculosis biomarker detection. (a) Schematic of a Tube^2 field effect point sensor immersed in a drop of biofluid containing IS6110. (b) Photograph of Tube^2 field effect point sensors fabricated from a metal−silicon−metal wafer (inset) by a simple dice-and-dip procedure. Note that the paratrechina flavipes ant that is exploring has a size similar to the sensors (3.5 mm × 0.5 mm × 20 μm). (c) I−V curves of a representative Tube^2 field effect point sensor in response to IS6110. Inset shows the sequences of the probe DNA and IS6110. (d) Current change of a representative Tube^2 field effect point sensor when exposed to various concentrations of IS6110 (red, target) and 5′-$(TAT)_5$-3′ (dark blue, 11 out of 15 mismatches). The sensors are operated at a source−drain voltage of 0.1 V, without a physical gate. The black dotted line indicates the current level equivalent to 3 times the noise, which is defined as the current fluctuation in 10 mM PBS control solution without any DNA.

TFTs were evaluated by differences in conductance when exposed to a noncomplementary DNA sequence (ncDNA) versus the cDNA sequence. Addition of ncDNA sequences with single (5′-AAC GTG AGT CGC CTA TCC ACT AT-3′), double (5′-AAC GT**T** AGT CGC CTA TCC AC**T** AT-3′), and 13 mismatched bases (5′-/**TAT TAT TAT TAT TAT TT**T/-3′) showed progressively smaller conductance increase than the cDNA (Figure 3e). Single-mismatch selectivity, at nanomolar concentrations and throughout the large concentration range tested, can be achieved without the use of an external gate and any amplification techniques. These experiments clearly show that chemically gated Tube^2 TFTs possess simultaneous high sensitivity and selectivity similar to their electrode-gated counterparts, which have further shown that when combined with amplification techniques, femtomolar detection of oligonucleotides can be achieved.[31,32]

For futher verification that electrostatic/chemical gating is the dominant sensing mechanism, oligonucleotide length dependence studies were performed. In support of this hypothesis, longer ssDNA sequences, which have more negative charge, generate larger chemical gating effects and signal response upon hybridization due to a larger amount of bound charge. By increasing the ssDNA probe and cDNA target from 10 to 23 bases, the projected detection limit improved by approximately 40%, and the concentration dependence on V_{th} shift (the slope) decreased by a factor of about 2.5 (Figure S4). Furthermore, Tube^2 TFTs can be reused multiple times by heating at 95 °C to dehybridize bound oligonucleotides from their probe sequences followed by displacement of free oligonucleotides by copious rinsing. The devices also show excellent long-term stability of their electrical properties up to 9 months stored in a desiccator.

To test the feasibility of the chemically gated Tube^2 TFT platform for detecting realistic targets, we demonstrate the detection of the 123-base *Mycobacterium tuberculosis* biomarker (IS6110). Although tuberculosis is treatable, its extremely high transmission rate and few symptoms cause it to result in approximately 1.5 million deaths annually worldwide. Current diagnostic methods are either low in sensitivity (only 34−80%, sputum smear microscopy), time-consuming (requires 9−16 days for culture of bacilli), or too sophisticated (molecular species diagnostics) to be adopted for developing countries. Furthermore, a majority of newly infected cases are in the developing countries, meaning a rapid, simple, low cost, and highly accurate on-site detection platform for early diagnosis can have a great positive impact on public health. To detect

DOI: 10.1021/jacs.6b12111
J. Am. Chem. Soc. 2017, 139, 3045−3051

IS6110, a 15-base amino-modified ssDNA probe (/5AmMC6/ GC GAG CGT AGG CGT C) that is complementary at the 3′ end of one of the IS6110 DNA strands was linked to the functionalized Tube^2 devices. The IS6110 double-stranded DNA (dsDNA) was dehybridized by melting and immediately dispensed through the ssDNA-modified TFTs using microfluid channels. Upon addition of the IS6110 marker, similar to the binding of the model 23-base cDNA, chemical gating shifts in transport properties that resulted in an increase in conductance were observed (Figure S5). This is consistent with specific IS6110 attachment to the probe-modified Tube^2 TFT.

Without the need for a third electrode and a dielectric, a Tube^2 field effect sensor can be fabricated as a free-standing point probe with only source/drain electrodes (Figure 4a). To demonstrate the functionality gained through eliminating a physical gate electrode, a two-terminal field effect point sensor was created using a photolithography-free, high throughput dice-and-dip procedure (Figure S6). Electrodes are easily fabricated by double-sided deposition of gold on an undoped silicon wafer, and individual devices are mass produced by dicing the metal−silicon−metal wafer into millimeter scale pieces (Figure 4b). The channel length (20 μm) of the device is defined directly by the cross-sectional thickness of the Si wafer. Tube^2 sensing devices are created in parallel by self-assembling DWCNT networks across the cross-section of the wafers followed by diazonium functionalization and oligonucleotide coupling. The overall conductivity between point sensors varied more than that of the traditionally fabricated TFTs, which may arise due to varying Tube^2 densities and network morphologies from the dice-and-dip procedure; however, for a set of 24 point sensors, all readily achieved submicromolar sensitivity for IS6110 and selectivity over other mismatched oligonucleotide sequences, closely matching the performance of microfabricated on-chip devices (Figure 4c,d and Figure S7).

CONCLUSIONS

We demonstrated that Tube^2 semiconductors can be gated solely by chemically attached groups enabling gate electrode-free thin film transistor sensors. Two-terminal thin film transistor sensors were shown to reach nanomolar detection limits toward the detection of a 23-base cDNA sequence, while simultaneously achieving single base mismatch selectivity. Our chemically gated TFT sensors have also demonstrated the ability to detect IS6110, a known DNA biomarker of tuberculosis. The ability to fabricate a high performance field effect sensor without a gate electrode enabled the creation of a photolithography-free, high throughput Tube^2 point sensor with FET sensitivity and selectivity, but using a two-terminal configuration that is as simple as a chemiresistor[10,12−15] and significantly simplified compared to the conventional three-terminal FET sensors. This two-terminal FET sensor architecture is readily compatible with other versatile fabrication techniques such as paper electronics[33] and lab-on-a-chip devices[34] to maximize the portable, real-time, and label-free advantages of electrical sensing. Prototypical devices have shown detection limits of oligonucleotides and tuberculosis biomarkers comparable to state-of-the-art three-terminal counterparts that are physically gated.[31,35] This new concept thus may open up new opportunities for materials chemistry and device innovation.

ASSOCIATED CONTENT

Supporting Information

The Supporting Information is available free of charge on the ACS Publications website at DOI: 10.1021/jacs.6b12111.

Additional experimental details, electrical transport measurements, IR spectra, pH dependence, and base pair dependence (PDF)

AUTHOR INFORMATION

Corresponding Author

*yhw@umd.edu

ORCID

Zhiwei Peng: 0000-0002-8278-2565

YuHuang Wang: 0000-0002-5664-1849

Notes

The authors declare no competing financial interest.

ACKNOWLEDGMENTS

Research reported in this publication was supported by the National Institute of General Medical Sciences of the National Institutes of Health under Award Number R01GM114167. We also gratefully acknowledge the National Science Foundation for partial support through Grant CHE-1507974 on the development of the surface chemistry. We acknowledge the Maryland NanoCenter and its FabLab for assistance with microfabrication. The authors also gratefully acknowledge M. C. Hersam and A. Green for assistance with DGU, P. Wang for help with schematic illustrations, C. F. Sun for SEM imaging, and B. Meany for discussions.

REFERENCES

(1) Choi, Y. K.; Moody, I. S.; Sims, P. C.; Hunt, S. R.; Corso, B. L.; Perez, I.; Weiss, G. A.; Collins, P. G. *Science* **2012**, *335*, 319.

(2) Munzer, A. M.; Michael, Z. R.; Star, A. *ACS Nano* **2013**, *7*, 7448.

(3) Patolsky, F.; Zheng, G.; Lieber, C. M. *Nanomedicine* **2006**, *1*, 51.

(4) Penner, R. M. *Annu. Rev. Anal. Chem.* **2012**, *5*, 461.

(5) Rajan, N. K.; Duan, X. X.; Reed, M. A. *Wiley Interdiscip. Rev. Nanomed. Nanobiotechnol.* **2013**, *5*, 629.

(6) Mackay, I. M.; Arden, K. E.; Nitsche, A. *Nucleic Acids Res.* **2002**, *30*, 1292.

(7) Mor, G.; Visintin, I.; Lai, Y.; Zhao, H.; Schwartz, P.; Rutherford, T.; Yue, L.; Bray-Ward, P.; Ward, D. C. *Proc. Natl. Acad. Sci. U. S. A.* **2005**, *102*, 7677.

(8) Stern, E.; Klemic, J. F.; Routenberg, D. A.; Wyrembak, P. N.; Turner-Evans, D. B.; Hamilton, A. D.; LaVan, D. A.; Fahmy, T. M.; Reed, M. A. *Nature* **2007**, *445*, 519.

(9) Snow, E. S.; Perkins, F. K.; Robinson, J. A. *Chem. Soc. Rev.* **2006**, *35*, 790.

(10) Wang, F.; Swager, T. M. *J. Am. Chem. Soc.* **2011**, *133*, 11181.

(11) Abdellah, A.; Abdelhalim, A.; Horn, M.; Scarpa, G.; Lugli, P. *IEEE Trans. Nanotechnol.* **2013**, *12*, 174.

(12) Wang, F.; Gu, H. W.; Swager, T. M. *J. Am. Chem. Soc.* **2008**, *130*, 5392.

(13) Ammu, S.; Dua, V.; Agnihotra, S. R.; Surwade, S. P.; Phulgirkar, A.; Patel, S.; Manohar, S. K. *J. Am. Chem. Soc.* **2012**, *134*, 4553.

(14) Fennell, J. F.; Liu, S. F.; Azzarelli, J. M.; Weis, J. G.; Rochat, S.; Mirica, K. A.; Ravnsbaek, J. B.; Swager, T. M. *Angew. Chem., Int. Ed.* **2016**, *55*, 1266.

(15) Ishihara, S.; Azzarelli, J. M.; Krikorian, M.; Swager, T. M. *J. Am. Chem. Soc.* **2016**, *138*, 8221.

(16) Green, A. A.; Hersam, M. C. *Nat. Nanotechnol.* **2009**, *4*, 64.

(17) Moore, K. E.; Tune, D. D.; Flavel, B. S. *Adv. Mater.* **2015**, *27*, 3105.

(18) Cao, Q.; Rogers, J. A. *Adv. Mater.* **2009**, *21*, 29.

DOI: 10.1021/jacs.6b12111
J. Am. Chem. Soc. 2017, 139, 3045−3051

(19) Sun, D. M.; Timmermans, M. Y.; Tian, Y.; Nasibulin, A. G.; Kauppinen, E. I.; Kishimoto, S.; Mizutani, T.; Ohno, Y. *Nat. Nanotechnol.* **2011**, *6*, 156.
(20) Ng, A. L.; Sun, Y.; Powell, L.; Sun, C. F.; Chen, C. F.; Lee, C. S.; Wang, Y. H. *Small* **2015**, *11*, 96.
(21) Huang, J.; Ng, A. L.; Piao, Y. M.; Chen, C. F.; Green, A. A.; Sun, C. F.; Hersam, M. C.; Lee, C. S.; Wang, Y. H. *J. Am. Chem. Soc.* **2013**, *135*, 2306.
(22) Piao, Y. M.; Chen, C. F.; Green, A. A.; Kwon, H.; Hersam, M. C.; Lee, C. S.; Schatz, G. C.; Wang, Y. H. *J. Phys. Chem. Lett.* **2011**, *2*, 1577.
(23) Bahr, J. L.; Yang, J. P.; Kosynkin, D. V.; Bronikowski, M. J.; Smalley, R. E.; Tour, J. M. *J. Am. Chem. Soc.* **2001**, *123*, 6536.
(24) Shih, C. J.; Wang, Q. H.; Jin, Z.; Paulus, G. L. C.; Blankschtein, D.; Jarillo-Herrero, P.; Strano, M. S. *Nano Lett.* **2013**, *13*, 809.
(25) Bouilly, D.; Cabana, J.; Meunier, F.; Desjardins-Carriere, M.; Lapointe, F.; Gagnon, P.; Larouche, F. L.; Adam, E.; Paillet, M.; Martel, R. *ACS Nano* **2011**, *5*, 4927.
(26) Ren, W.; Reimers, J. R.; Hush, N. S.; Zhu, Y.; Wang, J.; Guo, H. *J. Phys. Chem. C* **2007**, *111*, 3700.
(27) Schmidt, G.; Gallon, S.; Esnouf, S.; Bourgoin, J. P.; Chenevier, P. *Chem. - Eur. J.* **2009**, *15*, 2101.
(28) Heller, I.; Janssens, A. M.; Mannik, J.; Minot, E. D.; Lemay, S. G.; Dekker, C. *Nano Lett.* **2008**, *8*, 591.
(29) Mahshid, S. S.; Camire, S.; Ricci, F.; Vallee-Belisle, A. *J. Am. Chem. Soc.* **2015**, *137*, 15596.
(30) Park, M. H.; Han, D.; Chand, R.; Lee, D. H.; Kim, Y. S. *J. Phys. Chem. C* **2016**, *120*, 4854.
(31) Dong, X. C.; Lau, C. M.; Lohani, A.; Mhaisalkar, S. G.; Kasim, J.; Shen, Z. X.; Ho, X. N.; Rogers, J. A.; Li, L. J. *Adv. Mater.* **2008**, *20*, 2389.
(32) Star, A.; Tu, E.; Niemann, J.; Gabriel, J. C. P.; Joiner, C. S.; Valcke, C. *Proc. Natl. Acad. Sci. U. S. A.* **2006**, *103*, 921.
(33) Hamedi, M. M.; Ainla, A.; Guder, F.; Christodouleas, D. C.; Fernandez-Abedul, M. T.; Whitesides, G. M. *Adv. Mater.* **2016**, *28*, 5054.
(34) Laksanasopin, T.; Guo, T. W.; Nayak, S.; Sridhara, A. A.; Xie, S.; Olowookere, O. O.; Cadinu, P.; Meng, F. X.; Chee, N. H.; Kim, J.; Chin, C. D.; Munyazesa, E.; Mugwaneza, P.; Rai, A. J.; Mugisha, V.; Castro, A. R.; Steinmiller, D.; Linder, V.; Justman, J. E.; Nsanzimana, S.; Sia, S. K. *Sci. Transl. Med.* **2015**, *7*, 273re1.
(35) White, S. P.; Dorfman, K. D.; Frisbie, C. D. *Anal. Chem.* **2015**, *87*, 1861.

DOI: 10.1021/jacs.6b12111
J. Am. Chem. Soc. 2017, 139, 3045−3051